ENVIRONMENTAL RESEARCH
LETTERS

LETTER

Methane emission hotspots in a boreal forest-fen mosaic potentially linked to deep taliks

Mary Farina[1,*] , William Christian[2,3] , Nicholas Hasson[4] , Timothy McDermott[1] , Scott Powell[1] ,
Roland Hatzenpichler[2,3,5,6] , Hailey Webb[7,8] , Gage LaRue[2], Kyoko Okano[9], Eric A Sproles[10,11]
and Jennifer D Watts[1,12]

1   Department of Land Resources and Environmental Sciences, Montana State University, Bozeman, MT, United States of America
2   Department of Chemistry and Biochemistry, Montana State University, Bozeman, MT, United States of America
3   Center for Biofilm Engineering, Montana State University, Bozeman, MT, United States of America
4   Water and Environmental Research Center, University of Alaska Fairbanks, Fairbanks, AK, United States of America
5   Department of Microbiology and Cell Biology, Montana State University, Bozeman, MT, United States of America
6   Thermal Biology Institute, Montana State University, Bozeman, MT, United States of America
7   Department of Ecology and Evolutionary Biology, University of Colorado Boulder, Boulder, CO, United States of America
8   Renewable and Sustainable Energy Institute, University of Colorado Boulder, Boulder, CO, United States of America
9   Department of Biology and Wildlife, University of Alaska Fairbanks, Fairbanks, AK, United States of America
10   Department of Earth Sciences, Montana State University, Bozeman, MT, United States of America
11   Geospatial Core Facility, Montana State University, Bozeman, MT, United States of America
12   Woodwell Climate Research Center, Falmouth, MA, United States of America
*   Author to whom any correspondence should be addressed.

E-mail: mary.farina@student.montana.edu

Abstract

Permafrost thaw is transforming boreal forests into mosaics of wetlands and drier uplands. Topographic controls on hydrological and ecological conditions impact methane (CH_4) fluxes, contributing to uncertainty in local and regional CH_4 budgets and underlying drivers. The objective of this study was to explore CH_4 fluxes and their drivers in a transitioning boreal forest-fen ecosystem (Goldstream Valley, Alaska, USA). This landscape is characterized by thawing discontinuous permafrost and heterogeneous mosaics of fens, collapse-scar channels, and small mounds of permafrost soils. From a survey in July 2021, observed chamber CH_4 fluxes included fen areas with intermediate to very high emissions (29.8–635.3 mg CH_4 m^{-2} d^{-1}), clustered locations with CH_4 uptake (-2.11 to -0.7 mg CH_4 m^{-2} d^{-1}), and three anomalous emission hotspots (342.4–772.4 mg CH_4 m^{-2} d^{-1}) that were located near samples with lower emissions. Some surface and near-surface variables partially explained the spatial variation in CH_4 flux. Log-transformed CH_4 flux had a positive linear relationship with soil moisture at 20 cm depth ($R^2 = 0.31$, p-value $< 1e-5$) and negative linear relationships with microtopography ($R^2 = 0.13$, p-value < 0.006) and slope ($R^2 = 0.28$, p-value $< 2e-5$). Methane emissions generally occurred in flat, wet, graminoid-dominated fens, whereas CH_4 uptake occurred on permafrost mounds dominated by feather mosses and woody vegetation. However, the CH_4 hotspots occurred on drier, slightly sloped locations with low or undetectable near-surface methanogen abundance, suggesting that CH_4 was produced in deeper soils. When the hotspot samples were omitted, log-transformed CH_4 flux had a positive linear relationship with near-surface methanogen abundance ($R^2 = 0.29$, p-value $= 0.0023$), and stronger linear relationships with soil moisture, slope, and soil macronutrient concentrations. Our findings suggest that some CH_4 emission hotspots could arise from CH_4 in deep taliks. The inference that methanogenesis occurs in deep taliks was strengthened

by the identification of intrapermafrost taliks across the study area using low-frequency geophysical induction. This study assesses surface spatial heterogeneity in the context of subsurface permafrost conditions and highlights the complexity of CH_4 flux patterns in transitioning forest-wetland ecosystems. To better inform regional CH_4 budgets, further research is needed to understand the spatial distribution of terrestrial CH_4 hotspots and to resolve their surface, near-surface, and subsurface drivers.

1. Introduction

Methane (CH_4) has a high warming potential, and increases in atmospheric CH_4 have contributed $\sim$0.5 °C of global warming since the pre-industrial era (Myhre *et al* 2014, Masson-Delmotte *et al* 2021). Although wetlands comprise only 13% of the northern high-latitude terrestrial area (Olefeldt *et al* 2021), they are thought to be substantial biogenic CH_4 sources. Northern high-latitude CH_4 budgets are estimated to range from 11 to 53 Tg CH_4 yr^{-1}, and they are uncertain at local and regional scales, as shown by substantial disagreement among process-based models and atmospheric inversions (Saunois *et al* 2020, Bruhwiler *et al* 2021, Watts *et al* 2023, Hugelius *et al* 2024, Ying *et al* 2024). Much of the uncertainty stems from the challenge of process representation in ecosystem models to accurately predict rates of CH_4 production and oxidation, including the difficulty of accounting for subsurface permafrost conditions and spatial heterogeneity within coarse (1–500 km^2) grid cells (Douglas *et al* 2016, Oh *et al* 2020, Saunois *et al* 2020, Bruhwiler *et al* 2021). Net CH_4 fluxes are heterogeneous within and across high-latitude ecosystem types due to complex, spatiotemporally varying biotic and abiotic drivers that control CH_4 production and oxidation, including soil thaw depth, temperature, soil moisture, microbial community composition, vegetation, and soil organic carbon (SOC) content (Olefeldt *et al* 2013, Treat *et al* 2015, Kuhn *et al* 2021).

Northern high-latitude regions are rapidly warming (Rantanen *et al* 2022), and permafrost soils are thawing gradually through progressive active layer deepening, or abruptly through rapid losses of ice that lead to ground subsidence (thermokarst) (Turetsky *et al* 2020). Methane fluxes are impacted as ecosystems transition in response to warming and thaw. Boreal forests underlain by warm (-0.7 °C to -0.2 °C) discontinuous permafrost are especially susceptible to thermokarst (Osterkamp *et al* 2000, Lara *et al* 2016). As boreal forests transition into forest-wetland mosaics, they can switch from CH_4 sinks to sources (Helbig *et al* 2017, Kuhn *et al* 2021). Both methanogenesis and methanotrophy are positively related to temperature, and these temperature responses are mediated by soil moisture and other environmental factors, thus complicating our understanding of how net CH_4 flux responds to warming (Dunfield *et al* 1993, Peltoniemi *et al* 2016, Zhang *et al*

2021). In general, warming temperatures are thought to increase CH_4 emissions in high-latitude ecosystems, raising concerns about permafrost carbon feedbacks (Olefeldt *et al* 2013, Zhang *et al* 2017, Oh *et al* 2020, Wang *et al* 2024).

Water table depth is closely linked to microtopography, and together they control vertical soil moisture gradients and the extents of oxic and anoxic soil zones, thus affecting rates of CH_4 production and oxidation over fine spatial scales ($<$1 m^2) (Bubier *et al* 1993, Turetsky *et al* 2008, Juottonen *et al* 2015, Graham *et al* 2022). In boreal peatlands, *Sphagnum* hummocks (small mounds) have deeper water tables, larger oxic zones, and lower rates of CH_4 production relative to surrounding hollows (Bubier *et al* 1993, Frenzel and Karofeld 2000, Dorodnikov *et al* 2013). Thermokarst-affected boreal forests can also contain microtopography features and associated variation in soil moisture conditions, including well-drained permafrost mounds surrounded by wetter thaw depressions (Osterkamp *et al* 2000, Jorgenson and Osterkamp 2005).

Soil microbial communities are metabolically diverse and foundational to nutrient cycling and decomposition of SOC (Dubey *et al* 2021, Wagg *et al* 2021). Vertical and horizontal variations in CH_4-cycling microbial communities are driven by temperature, redox potential, substrate quality, nutrient availability, vegetation cover, soil pH, and other physicochemical conditions (Galand *et al* 2002, 2003, Kolb 2009, Andersen *et al* 2013, Juottonen *et al* 2015). Methanogens are thought to be more abundant below the water table (Chapman *et al* 2017), whereas soils closer to the surface can benefit aerobic methanotrophic bacteria due to the presence of both CH_4 and oxygen (Andersen *et al* 2013). Across a thaw gradient in the Tanana River floodplain (interior Alaska, USA), methanogen abundance and potential CH_4 production were higher in collapse-scar bogs relative to forested bogs with intact permafrost (Chapman *et al* 2017).

Vegetation composition is another important driver of high-latitude CH_4 fluxes (Olefeldt *et al* 2013). Wetland-adapted vascular plants have hollow tissues (aerenchyma) that facilitate oxygen diffusion to the rhizosphere, promoting CH_4 oxidation. However, CH_4 produced in saturated soil can diffuse upward through aerenchyma, bypassing the oxic soil zone and increasing net emissions (Turetsky *et al* 2014). Plants also supply litter and root exudates

that provide substrates for methanogenesis (Zhang *et al* 2021). Although the net result of these factors is site-specific (Rupp *et al* 2019), synthesis studies have shown that graminoid-dominated wetlands tend to have high CH_4 emissions at the ecosystem level (Turetsky *et al* 2014, Bao *et al* 2021, Zhang *et al* 2021). Graminoids can contribute to high emissions by providing labile substrates for methanogens and by transporting CH_4 through well-developed aerenchyma.

Permafrost thaw increasingly exposes older, deeper SOC to decomposition and release to the atmosphere (Dorrepaal *et al* 2009, Schuur *et al* 2015, Waldrop *et al* 2021). Recent studies in interior Alaska used novel geophysical methods and *in situ* observations to find that taliks (perennially thawed bulbs above or inside permafrost) underlying an abrupt-thaw thermokarst lake are likely contributing to lake and nearshore CH_4 emission hotspots (Elder *et al* 2021, Walter Anthony *et al* 2021). Other geophysical studies in interior Alaska assessed permafrost structure and CH_4 in the context of soil microbial, geochemical, and moisture profiles, providing evidence of methanogenesis in deep thaw zones in terrestrial thermokarst environments (Douglas *et al* 2016, James *et al* 2021, Walter Anthony *et al* 2024). At the regional scale, CH_4 hotspots are associated with high thermokarst occurrence (Elder *et al* 2021).

Our objectives were to assess spatial variation in CH_4 flux and identify its key environmental drivers in a transitioning boreal forest-fen ecosystem underlain by thawing discontinuous permafrost. To do this, we combined *in situ* observations of chamber CH_4 fluxes and soil conditions; analysis of soil microbial communities and soil chemistry; terrain and vegetation modeling; and geophysical characterization of permafrost structure. We hypothesized that CH_4 flux would be strongly associated with surface and near-surface conditions, including soil moisture, soil temperature, soil chemical properties, vegetation cover, methanogen relative abundance, and terrain variables. We also hypothesized that deep permafrost thaw would contribute to high CH_4 emissions.

2. Methods

2.1. Study area

The study was conducted in a boreal forest-fen mosaic ecosystem in Goldstream Valley (GSV), a 100 km^2 watershed located 5 km north of Fairbanks, Alaska, USA (64.922° N, 147.821° W; figure 1). This region is underlain by discontinuous permafrost and contains abundant wetlands (Walter Anthony *et al* 2021). Mean annual air temperature is around -2 °C and has increased by $\sim$1.5 °C over the last century (Wendler and Shulski 2009, James *et al* 2021). Increases in temperature and precipitation have led to deeper active layers and widespread thermokarst in

recent decades (Douglas *et al* 2020, Walter Anthony *et al* 2021). Recent (*ca.* 2018) talik formation across the Alaskan discontinuous permafrost zone indicates widespread increases in active layer depth and incomplete winter refreezing, which leads to increased hydrological connectivity (Farquharson *et al* 2022). Increased groundwater flow can in turn enhance thaw through advective heat transfer (Walvoord and Kurylyk 2016, Farquharson *et al* 2022).

Permafrost in GSV has complex paleo-depositional structure, including unconformities between Yedoma (ice- and SOC-rich syngenetic permafrost that formed during the Pleistocene and remains abundant in parts of Alaska) and Holocene-aged epigenetic ice wedges (Kanevskiy *et al* 2022). The deposits of discontinuous, Holocene-aged, *reworked* Yedoma can be tens of meters thick (Walter Anthony *et al* 2021). Soils in the GSV valley center are primarily classified as Typic Histoturbels ('Goldstream series'), which consist of cold, poorly drained soils with thick organic layers ($>$20 cm) that formed on deep, reworked loess (Soil Survey Staff, Ping *et al* 2006).

We collected data in a transitioning forest-fen mosaic 150 m north of Big Trail Lake (BTL), an active thermokarst lake near the valley center (Walter Anthony *et al* 2021). Rivulet channels drain the fens to the southwest toward BTL ($\sim$0.2% slope). Such permafrost and relief conditions can foster complex microtopography and hydrology that create mosaics of permafrost-cored mounds and collapse-scar fens (Osterkamp *et al* 2000, Walvoord and Kurylyk 2016, Wright *et al* 2022). We note that, in addition to warming and hydrologic conditions, anthropogenic disturbances (such as the presence of an unpaved access road or the diverting of Goldstream Creek) might have contributed to the formation and expansion of thermokarst and talik features in this area (O'Neill *et al* 2020, Elder *et al* 2021).

Microtopography and vegetation are highly heterogeneous across the study area (SI figures 1–4). Fen areas are generally dominated by graminoids including blue joint grass (*Calamagrostis canadensis*), tussock cottongrass (*Eriophorum vaginatum*), and sedges (*Carex* spp.). Small permafrost mounds are generally dominated by feather mosses and woody vegetation including mixed trees and shrubs of willow (*Salix* spp.), spruce (*Picea* spp.), alder (*Alnus* spp.), birch (*Betula* spp.), and *Vaccinium* spp. Supplementary section SI.1 provides further details.

2.2. Methane flux data collection

Chamber estimates of net CH_4 flux were collected at 15 sites across a 2 ha area (figure 1) over a 6 d period in July 2021 (between 1100 and 1800 Alaska Daylight Time). The selection of the 15 sites was largely random, but we tried to cover a range of vegetation and soil moisture conditions present in the forest-fen ecosystem (SI figure 1). Fluxes were estimated at four
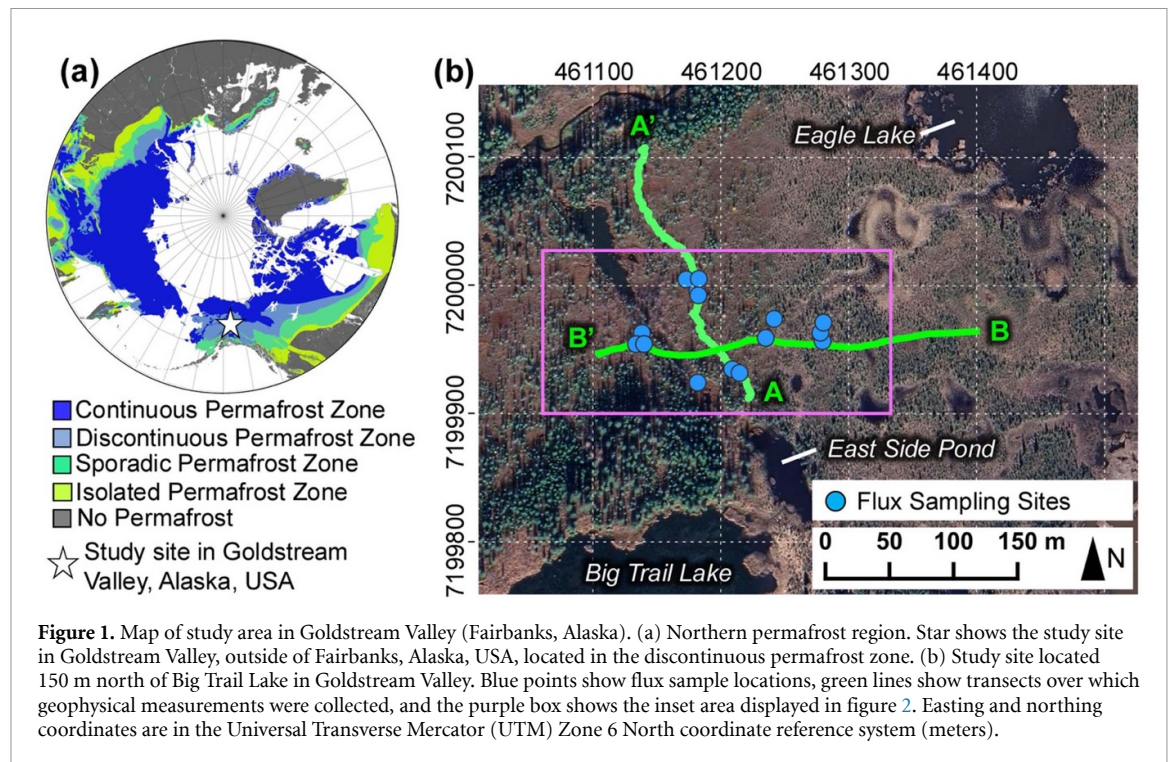
Figure 1. Map of study area in Goldstream Valley (Fairbanks, Alaska). (a) Northern permafrost region. Star shows the study site in Goldstream Valley, outside of Fairbanks, Alaska, USA, located in the discontinuous permafrost zone. (b) Study site located 150 m north of Big Trail Lake in Goldstream Valley. Blue points show flux sample locations, green lines show transects over which geophysical measurements were collected, and the purple box shows the inset area displayed in figure 2. Easting and northing coordinates are in the Universal Transverse Mercator (UTM) Zone 6 North coordinate reference system (meters).

sample locations within an average 4 m^2 area per site. However, fluxes were estimated at two locations at sites 8 and 9 due to the difficulty of flux collection at these very wet sites, giving a total of 56 sample locations. Fluxes were collected using a LI-7810 trace gas analyzer and 8200–01S Smart Chamber (LI-COR, Lincoln, NE, USA) placed on a cylindrical, polyvinyl chloride soil collar (10 cm diameter). Three replicate fluxes were estimated and averaged for each sample location. For each replicate, the Smart Chamber was placed on a soil collar, and the gas analyzer measured the change in CH_4 gas concentration in the chamber headspace during a 5 min closed-chamber period. Fluxes were computed using exponential or linear fits of the concentration data over time, and the quality of the flux estimates was evaluated based on R^2 values of the model fits (SoilFluxPro version 4.2.1). The fluxes were adjusted based on visual estimates of the percentage of chamber volume occupied by vegetation. Supplementary section SI.2 provides further details on the flux calculations and adjustments based on vegetation volumes.

The resulting mean CH_4 flux estimates were binned into five categories: very high [200, 722.4], high [100, 200), intermediate [10, 100), low (0, 10), and negative [−2.1, 0), thresholds in mg CH_4 m^{-2} d^{-1} (square brackets indicate inclusive endpoints and parentheses indicate exclusive endpoints).

2.3. Surface and near-surface (active layer) characterization

Vegetation composition was recorded at all 56 sample locations, with plants identified to species or genus

level when possible. The sample locations were classified into nine vegetation classes based on visual assessment of the cover of dominant plant types within soil collars: (1) moss, sedge, field horsetail; (2) sedge, grass, moss; (3) moss, field horsetail, grass, sedge; (4) variegated horsetail, moss, sedge; (5) grass, sedge, moss; (6) field horsetail, moss, grass, sedge; (7) moss, field horsetail; (8) dwarf shrub, moss, field horsetail, grass, sedge; and (9) moss. In each class name, the most dominant plant types are listed first. Vegetation across the study area was highly mixed and many sample locations contained similar types of vegetation in varying abundances. The classification was an attempt to differentiate vegetation conditions among the sample locations based on plant types and abundances. SI figure 2 shows example photographs for each class.

Near-surface (active layer) data was collected *in situ*, including soil moisture at 6, 12, and 20 cm depths using a Hydrosense II sensor (Campbell Scientific, Logan, UT, USA); soil temperature at 5 and 10 cm depths using a HI98331 GroLine probe (Hanna Instruments, Woonsocket, RI, USA); and soil pH at 2.5 and 6 cm depths using a HI981030 GroLine probe. Volumetric water content (VWC) was estimated by applying calibration equations developed for organic boreal soils (Bourgeau-Chavez *et al* 2025) to the Hydrosense II measurements of period. Soil samples were collected from a subset of 17 locations at four depths (0–13, 13–25, 25–38, 38–51 cm). Soil samples were transported to a soils lab at Montana State University on wet ice, where they were frozen at −80 °C for several months. In addition to microbial

community analysis (section 2.4), the soil samples were analyzed for general chemical properties, concentrations of macronutrients (nitrate, ammonium, phosphorus, potassium, calcium, magnesium, and sulfate concentration), and base cation saturation (Agvise Laboratories, Northwood, ND, USA).

Microtopography was modeled across the study area using the USGS 3D elevation program (3DEP) lidar-based digital terrain model (DTM; 0.5 m spatial resolution)(OCM Partners 2023) aggregated to 1 m spatial resolution. The local mean DTM elevation was calculated using a 31 by 31 m moving window, and per-grid cell microtopography was calculated as the local mean subtracted from the original DTM (SI figure 5; Rodenhizer *et al* 2022). A window size of 31 by 31 m was selected because the local means captured the broad elevation trend over the study area (i.e. slight elevation decline to the southwest), and the microtopography calculation largely removed this trend (SI figures 5–7). The DTM data was also used to model gridded slope based on 8-pixel neighborhoods.

In August 2019, drone imagery in the near-infrared (NIR), red, and green spectral bands (13 cm spatial resolution) was collected over the study area using a multiSPEC-4C sensor onboard an eBee drone (senseFly, Lausanne, Switzerland). In July 2021, imagery in the NIR, red edge, red, green, and blue spectral bands (9 cm spatial resolution) was collected using a RedEdge-MX sensor (MicaSense) onboard a SwitchBlade drone (Vision Aerial, Bozeman, MT, USA). The normalized difference vegetation index was calculated for both the multiSPEC-4C and RedEdge-MX data. A simplified set of land cover classes (graminoid, moss, woody vegetation, shadow, and surface water) was mapped over the study area using supervised random forest classification (500 trees, two variables per split). Details are provided in supplementary section SI.3.

2.4. Microbial community analysis
For the soil samples described in section 2.3, DNA was extracted using the Qiagen PowerSoil Pro kit. 16 S rRNA gene amplification, sequencing, and subsequent bioinformatics data analysis was done as described in Krukenberg *et al* (2021). Further details can be found in supplementary section SI.4. Briefly, the V4 hypervariable region of the 16 S rRNA genes was amplified using the 515 F and 806 R Earth Microbiome Project primers, allowing approximately genus-level resolution of most bacterial and archaeal taxa (Parada *et al* 2016, Thompson *et al* 2017). DNA sequencing was performed at the Molecular Research Core Facility at Idaho State University (Pocatello, ID). Sequences were deposited at NCBI's GenBank under BioProject PRJNA1053625. The amplicon sequencing data was processed using QIIME2 (Bolyen *et al* 2019) and merged using DADA2 (Callahan *et al* 2016). The resulting amplicon sequence variants (ASVs)

were assigned taxonomy using Silva138 (Quast *et al* 2012, Yilmaz *et al* 2014). A total of 1591 ASVs were recovered and 1463 ASVs were retained after removal of contaminants using the *R* package *decontam* (Davis *et al* 2018) and manual curation. Samples were rarified prior to diversity analysis to the lowest number of merged reads in any sample (47 088).

2.5. Statistical analysis
We assessed linear relationships between log-transformed CH_4 flux and driver variables. The CH_4 flux observations were log-transformed because the flux values were highly positively skewed. We used an alpha level of 0.05 to assess significance in linear relationships.

2.6. Electromagnetic (EM) surveys of permafrost conditions
Very low-frequency (VLF) methods utilize EM wavefields generated by powerful military transmitters (typically ∼1 MW). These signals propagate within the Earth–ionosphere waveguide as far-field plane waves. VLF wavefields are ideal for probing shallow to intermediate depths in the subsurface. The magneto-telluric plane-wave nature of these sources, operating at frequencies of 15–30 kHz, allows depths of investigation ranging from tens to hundreds of meters, depending on the EM frequency, local ground resistance, season, and substrate. Substrates such as permafrost allow greater depth of investigation. VLF has provided two-dimensional (2D) inversions of hydrogeophysical and environmental variables (McNeill and Labson 1991), particularly for groundwater investigations (Stewart and Bretnall 1986, Benson *et al* 1997, Monteiro Santos 2004, Liljedahl *et al* 2020), including permafrost regions (Hoekstra *et al* 1974, 1975, Liljedahl *et al* 2020). A review of VLF theory and practical applications can be found in McNeill and Labson (1991).

We utilized VLF of frequency-domain EM induction to derive resistivity (in Ohm m) to evaluate the horizontal and vertical extent of permafrost. VLF transects were conducted along two distances (200 m and 300 m). Data were collected using a GemSystem 19WV instrument (Gem Systems, Inc., Markham, Ontario, Canada), measuring EM diffusion velocity and phase angles (φ) from primary wavefields generated by the U.S. Navy (Tx, NPM) at a frequency of 21.4 kHz, with measurements recorded approximately every 6 m along transects. The transects were oriented approximately perpendicular (Transect A) and parallel (Transect B) to the hydrological flow down the valley (figure 1). Surveys were conducted in August 2022 between 1300 and 1800 Alaska Daylight Time. Elevation models were obtained using Digital Positioning Guidance System.

The VLF data were inverted to reconstruct resistivity models using the EMTOMO software (Santos

et al 2006). We employed the nonlinear, smoothness-constrained inversion algorithm VLF2Dmf (Santos *et al* 2006). This inversion technique is 2D and is based on the Occam technique for 2D magnetotelluric data inversions (Constable *et al* 1987, Sasaki 1989, 2001, deGroot-Hedlin *et al* 1990). Forward modeling in the VLF2DMF program is based on the finite-element method, with topography incorporated through a distribution of the finite element mesh. Further details are provided in supplementary section SI.5.

3. Results

3.1. Spatial variation in CH_4 sources and sinks

Observed CH_4 fluxes included wet fen areas with intermediate to very high emissions (29.8–635.3 mg CH_4 m^{-2} d^{-1}) and drier locations with CH_4 uptake (-2.11 to -0.7 mg CH_4 m^{-2} d^{-1}) (figure 2). The uptake fluxes were spatially clustered on small mounds, whereas the majority of high or very high fluxes were spatially clustered in broad fen areas. In total, six flux samples were 'very high' ($\geqslant 200$ mg CH_4 m^{-2} d^{-1}). Among these, three samples were located in wet fens (297.4–635.3 mg CH_4 m^{-2} d^{-1}), and the other three were considered to be anomalous hotspots (342.4–772.4 mg CH_4 m^{-2} d^{-1}; hereafter referred to as hotspots). The three hotspot samples (3 N, 4 S, 4 W) were located on drier, slightly sloped boundaries between mounds and fen channels. We considered these samples to be anomalous hotspots because they were not located in a typical CH_4-emitting environment and because they occurred near (within 1–2 m) samples with low or intermediate emissions.

3.2. Characterizing surface and near-surface (active layer) environmental controls on CH_4 flux

Log-transformed CH_4 flux had a positive linear relationship with soil moisture at 20 cm depth ($R^2 = 0.31$, p-value $< 1 \times 10^{-5}$) and negative linear relationships with microtopography ($R^2 = 0.13$, p-value $= 0.006$) and slope ($R^2 = 0.28$, p-value $< 2 \times 10^{-5}$) (figure 3, SI table 1). These associations were also present when the samples were grouped by vegetation class (figure 4). The sedge and grass-dominated class (vegetation class 2) had large CH_4 emissions and saturated soils (mean 70% VWC at 20 cm depth), with flat slopes and neutral to low microtopography. The samples dominated by dwarf shrubs and feather mosses (vegetation classes 7–9) were drier (mean 42% VWC at 20 cm depth) and had mostly CH_4 uptake, slightly steeper slopes, and elevated microtopography. SI figures 2 and 4 show the variation in CH_4 flux by vegetation class.

In contrast to the results above, the CH_4 emission hotspot locations were relatively sloped and well-drained (mean 48% VWC at 20 cm depth).

Log-transformed CH_4 flux had more significant linear relationships with soil moisture at 20 cm depth ($R^2 = 0.38$, p-value $= 8 \times 10^{-7}$) and slope ($R^2 = 0.32$, p-value $= 9.2 \times 10^{-6}$) when the three CH_4 hotspot samples were omitted from the regressions (figure 3, SI table 1).
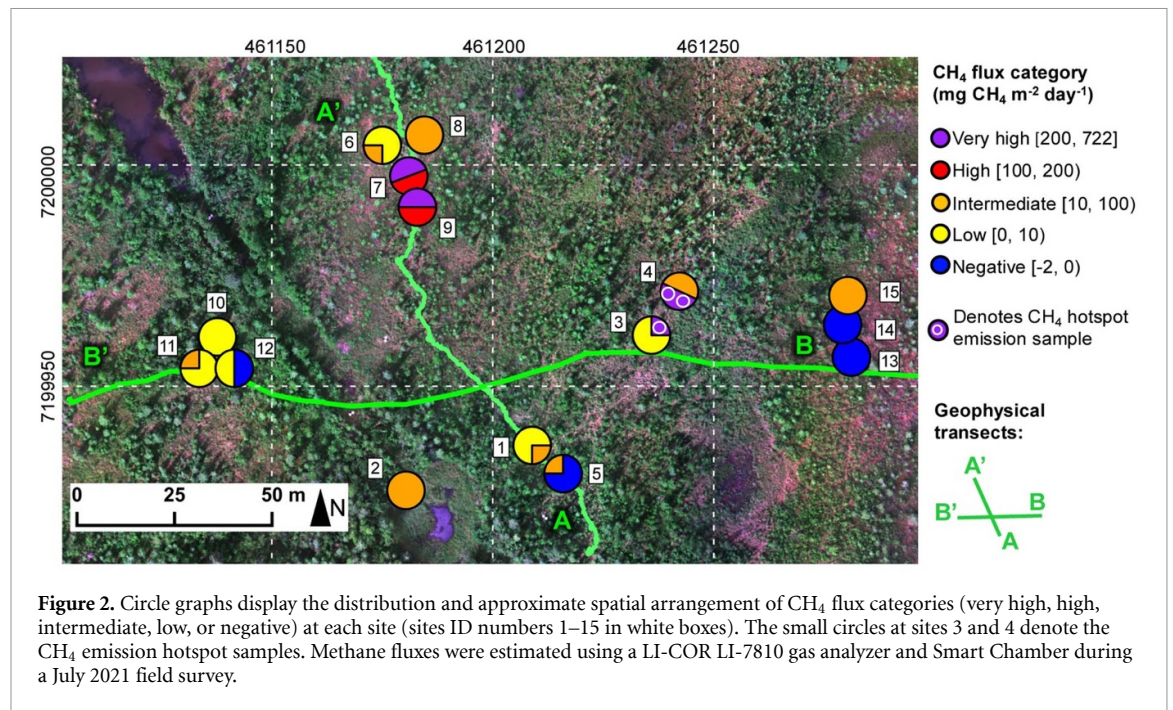
We did not observe significant relationships between log-transformed CH_4 flux and soil temperature or soil pH, when including or not including the hotspot samples (figure 3, SI table 1). We also did not observe a relationship between log-transformed CH_4 flux and air temperature from the stationary weather sensor, with or without the hotspots. Among the 17 locations where soil samples were collected, there was no relationship between log-transformed CH_4 flux and soil macronutrient concentrations. However, negative correlations between log-transformed CH_4 flux and some macronutrient variables became significant when the hotspot samples were omitted, including phosphorous, potassium, calcium, magnesium, and sulfate concentrations (SI table 1).

3.3. Influence of near-surface (active layer) microbial communities on CH_4 flux

Wet landscapes in permafrost regions are typically thought to emit large amounts of CH_4 due to the anaerobic degradation of SOC by archaeal methanogens. However, at the CH_4 hotspot locations, the relative abundance of methanogens was low or below detection (figure 5(a)). When considering all sample locations, we did not observe a significant relationship between natural log-transformed CH_4 flux and near-surface methanogen relative abundance, which is consistent with previous studies (reviewed in Kwon *et al* 2019). However, when the CH_4 flux hotspots were removed from regression analyses, there was a statistically significant positive correlation between methanogen relative abundance and CH_4 flux, including all sample depths ($R^2 = 0.198$, p-value < 0.01). This correlation was even stronger when only accounting for samples from 0–25 cm depth, with the hotspots still omitted ($R^2 = 0.29$, p-value $= 0.0023$, figure 5(a)).

Methanogen abundance and activity in permafrost environments rely on metabolic interactions with other organisms that provide substrates (syntrophy) for methanogenesis (hydrogen, acetate). Anaerobic fermentative cellulolytic bacteria such as *Clostridium* and *Acetobacterium* are known to be syntrophic partners to permafrost methanogens (Shcherbakova *et al* 2005, Tveit *et al* 2015, Fofana *et al* 2022), and were found to be significantly correlated with methanogens ($R^2 = 0.54$; p-value < 0.001) (figure 5(b)).

Methanotrophs use CH_4 as a carbon and energy source, and, as might be predicted, were most highly abundant in the CH_4 hotspot locations (figure 5(c)). Methanotroph relative abundance was correlated

Figure 2. Circle graphs display the distribution and approximate spatial arrangement of CH_4 flux categories (very high, high, intermediate, low, or negative) at each site (sites ID numbers 1–15 in white boxes). The small circles at sites 3 and 4 denote the CH_4 emission hotspot samples. Methane fluxes were estimated using a LI-COR LI-7810 gas analyzer and Smart Chamber during a July 2021 field survey.

with CH_4 flux across all samples and sites ($R^2 = 0.214$, p-value < 0.001, figure 5(c)). When the CH_4 hotspots were omitted from this regression, this relationship was still significant, although considerably weaker ($R^2 = 0.085$, p-value $= 0.018$).

3.4. Characterizing permafrost structure and subsurface controls on CH_4 flux

To characterize the permafrost spatially and vertically, we conducted 2D non-linear inversions of VLF data to generate resistivity models to 50 m depth. The inversions showed an upper permafrost table (0–10 m $\pm 2\sigma$ depth) composed of discontinuous, epigenetic permafrost (figure 6). This upper table contained high-resistivity features (>1000 Ohm m), interpreted as frozen permafrost, above and adjacent to areas with low resistivity (20–100 Ohm m), interpreted as intrapermafrost taliks (e.g. the low-resistivity areas at 7 m depth along Transect B at 170–260 m distance). The inversions also showed a lower permafrost table (10–50 m $\pm 10\sigma$ depth) composed of cold, continuous permafrost with high resistivity (2000–27 000 Ohm m). This lower table was interpreted to be dominated by syngenetic, foliated ice wedges (Yedoma), with no talik structures identified.

3.5. Modeled vegetation classes, microtopography, and slope across the geophysical transect

Figure 7 shows a portion of the Transect B geophysical inversion with the overlying CH_4 flux observations, microtopography, slope, and vegetation classes from the combined classification map (SI figure 14). Due to the challenge of precisely aligning the geophysical inversions with the other datasets, figure 7 shows the approximate spatial alignment of these datasets.

These results indicate that frozen permafrost features within the upper permafrost table are generally associated with higher microtopography, slope, and woody vegetation cover, whereas near-surface thawed areas are generally associated with flatter terrain and higher graminoid cover. Please note that the low-microtopography feature located at 220 m in figure 7 is related to an unpaved access road built in the mid twentieth century (Elder *et al* 2021).

4. Discussion

We observed CH_4 fluxes ranging from -2.11 to 772.4 mg CH_4 m^{-2} d^{-1}. A recent synthesis of Arctic-boreal wetland and upland sites reported mean daily warm-season chamber fluxes ranging from -10 to 705 mg CH_4 m^{-2} d^{-1}, with maximum daily fluxes exceeding 1000 mg CH_4 m^{-2} d^{-1} at some wetland sites (Kuhn *et al* 2021). Recent chamber flux measurements from the BTL littoral environment ($\sim$130 m from our sampling sites) are among the highest CH_4 fluxes reported for northern wetlands, ranging from 8.5 to 24 200 mg CH_4 m^{-2} d^{-1} (Elder *et al* 2021). In our study, the very high flux observations (up to almost 800 mg CH_4 m^{-2} d^{-1}) suggest that the forest-fen ecosystem surrounding the lake might also contribute substantially to regional CH_4 emissions, prompting us to investigate the key environmental variables driving the spatial variation in CH_4 flux.

Samples with high or very high CH_4 emissions mostly occurred in flat, wet, graminoid-dominated fens, which are typically considered to be CH_4-producing and emitting environments. However, in contrast to these results, three CH_4 hotspot samples were observed on drier, slightly sloped boundaries
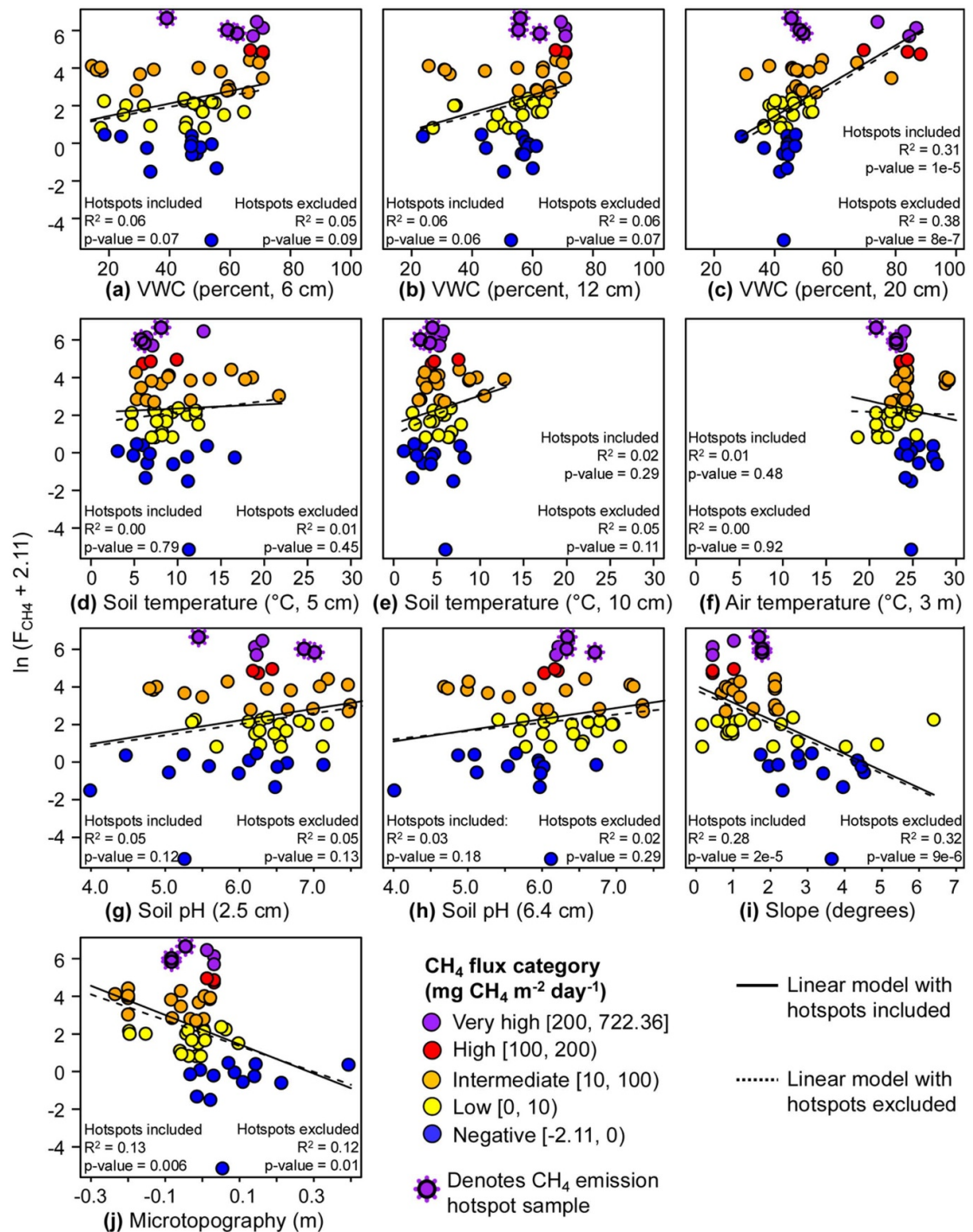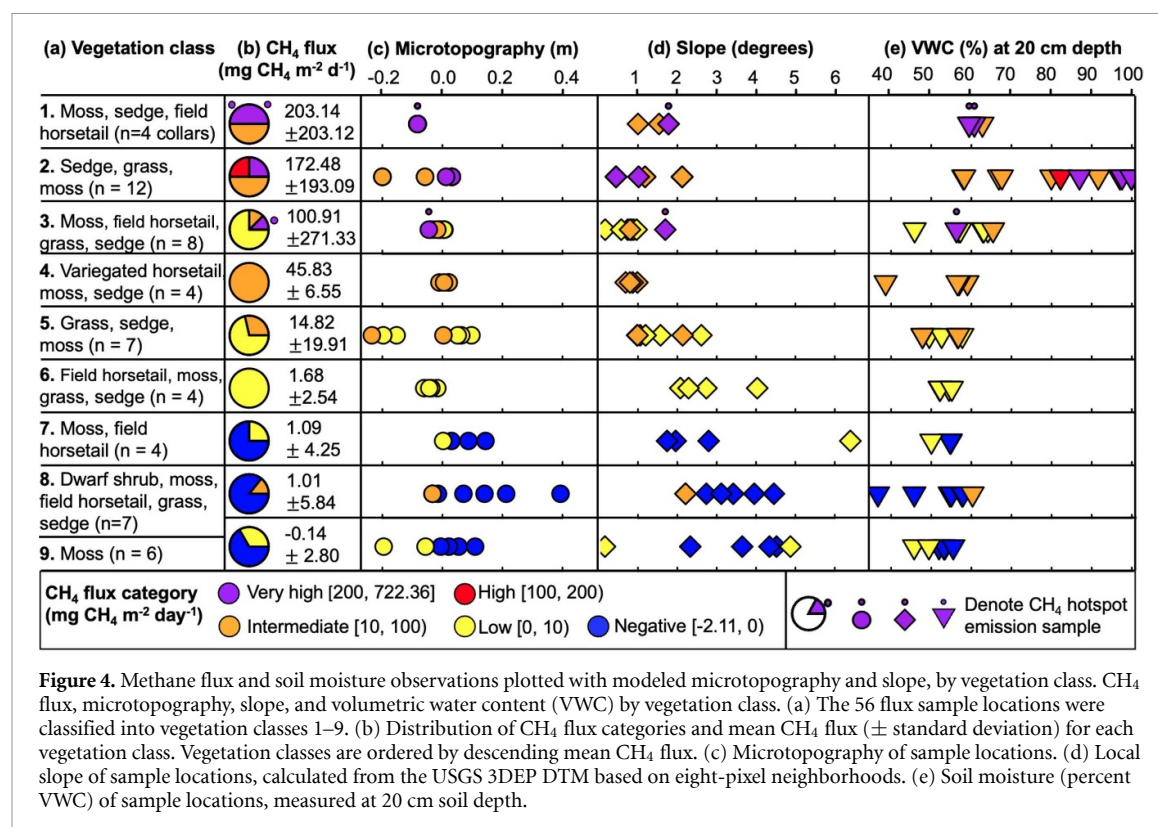
Figure 3. Methane flux observations plotted with (a)–(c) soil moisture at 6, 12, and 20 cm depths; (d)–(e) soil temperature at 5 and 10 cm depths; (f) air temperature at 3 m height; (g)–(h) soil pH at 2.5 and 6.4 cm depths; (i) modeled slope; and (j) modeled microtopography. Methane flux is plotted on the *y*-axes, expressed as $\ln(F_{CH4} + 2.11)$, in which F_{CH4} is the CH_4 flux in mg CH_4 m^{-2} day^{-1}. R^2 values and *p*-values are shown for the linear relationship between $\ln(F_{CH4} + 2.11)$ and each driver variable, with and without the CH_4 hotspot samples included.

between mounds and fens, located within 1–2 m of samples with low or intermediate emissions. These hotspot locations were moss-dominated, suggesting that the very high CH_4 emissions were not driven by plant-mediated transport. Moreover, methanogens were undetected or had low relative abundance in near-surface soils at the CH_4 hotspot locations, implying a deeper source of CH_4 (>50 cm depth).

These findings emphasize that information on deeper permafrost structure and thaw status is needed to understand the complete CH_4 budget (Douglas *et al* 2016).

The geophysical inversions showed an upper permafrost table with high-resistivity features, interpreted as frozen permafrost, above and adjacent to low-resistivity features, interpreted as

Figure 4. Methane flux and soil moisture observations plotted with modeled microtopography and slope, by vegetation class. CH_4 flux, microtopography, slope, and volumetric water content (VWC) by vegetation class. (a) The 56 flux sample locations were classified into vegetation classes 1–9. (b) Distribution of CH_4 flux categories and mean CH_4 flux ($\pm$ standard deviation) for each vegetation class. Vegetation classes are ordered by descending mean CH_4 flux. (c) Microtopography of sample locations. (d) Local slope of sample locations, calculated from the USGS 3DEP DTM based on eight-pixel neighborhoods. (e) Soil moisture (percent VWC) of sample locations, measured at 20 cm soil depth.

intrapermafrost taliks. The inversions also showed a lower permafrost table, interpreted as Yedoma. Extensive borehole and age dating records from GSV support these interpretations (Péwé 1958, 1975a, 1975b, Sellmann 1967). Previous studies have identified the upper table as the organic-rich, Holocene-aged Ready Bullion Formation (Qrb) and the lower table as the Pleistocene-aged Goldstream Formation (Qgs) (Péwé 1975a, 1975b, Hamilton *et al* 1988, Kanevskiy *et al* 2022). Supplementary section SI.5 provides further details on the Qrb and Qgs formations. Figure 7 shows that frozen Qrb permafrost features are associated with higher microtopography, slope, and woody vegetation cover, whereas near-surface thawed areas are associated with flatter terrain and higher graminoid cover. This is consistent with recent geophysical surveys in the Tanana Flats lowlands (southwest of Fairbanks), which found strong associations among vegetation, topography, thaw depth, and permafrost extent, with permafrost almost always present under forests and almost always absent under wetlands (Douglas *et al* 2016).

The geophysical results suggest that the upper permafrost table contains widespread taliks composed of saturated soils that might host methanogenesis. For example, the hotspot emissions at Site 3 might be explained by CH_4 produced in the underlying talik at $\sim$7 m depth and transported through thawed soils surrounding the Qrb permafrost feature (figure 6). Elder *et al* (2021) observed CH_4 hotspots in the BTL littoral zone near the edge of a

talik, likely driven by enhanced methanogenic production in deeper soils and/or by increased CH_4 channeling through the talik. Results of the current study suggest that a similar process occurs in the forest-fen ecosystem farther from the lake. Moreover, Walter Anthony *et al* (2024) observed large CH_4 emissions ($>$700 mg CH_4 m^{-2} d^{-1}) from thermokarst mound features at a thawing-Yedoma, non-wetland site in interior Alaska. Using borehole soil profiles, they observed higher water saturation, CH_4 concentration, and methanogen abundance at depth ($\geqslant$200 cm), indicating that methanogenesis occurs in deep taliks.

Our results also suggest that relationships between CH_4 flux and some surface or near-surface drivers were confounded by the three CH_4 hotspots. When the hotspots were omitted from regression analyses, relationships between log-transformed CH_4 flux and methanogen relative abundance and some soil macronutrient concentrations became evident, and relationships between log-transformed CH_4 flux and slope and soil moisture at 20 cm became slightly more significant (figures 3 and 5, SI table 1). This suggests that deeper subsurface conditions contribute to spatial variation in CH_4 flux by giving rise to emission hotspots, obscuring otherwise important relationships between CH_4 flux and surface and near-surface drivers (see figure 8 for a conceptual illustration). Although the CH_4 hotspot samples might be driven by deep subsurface conditions, the other samples were likely more influenced by surface
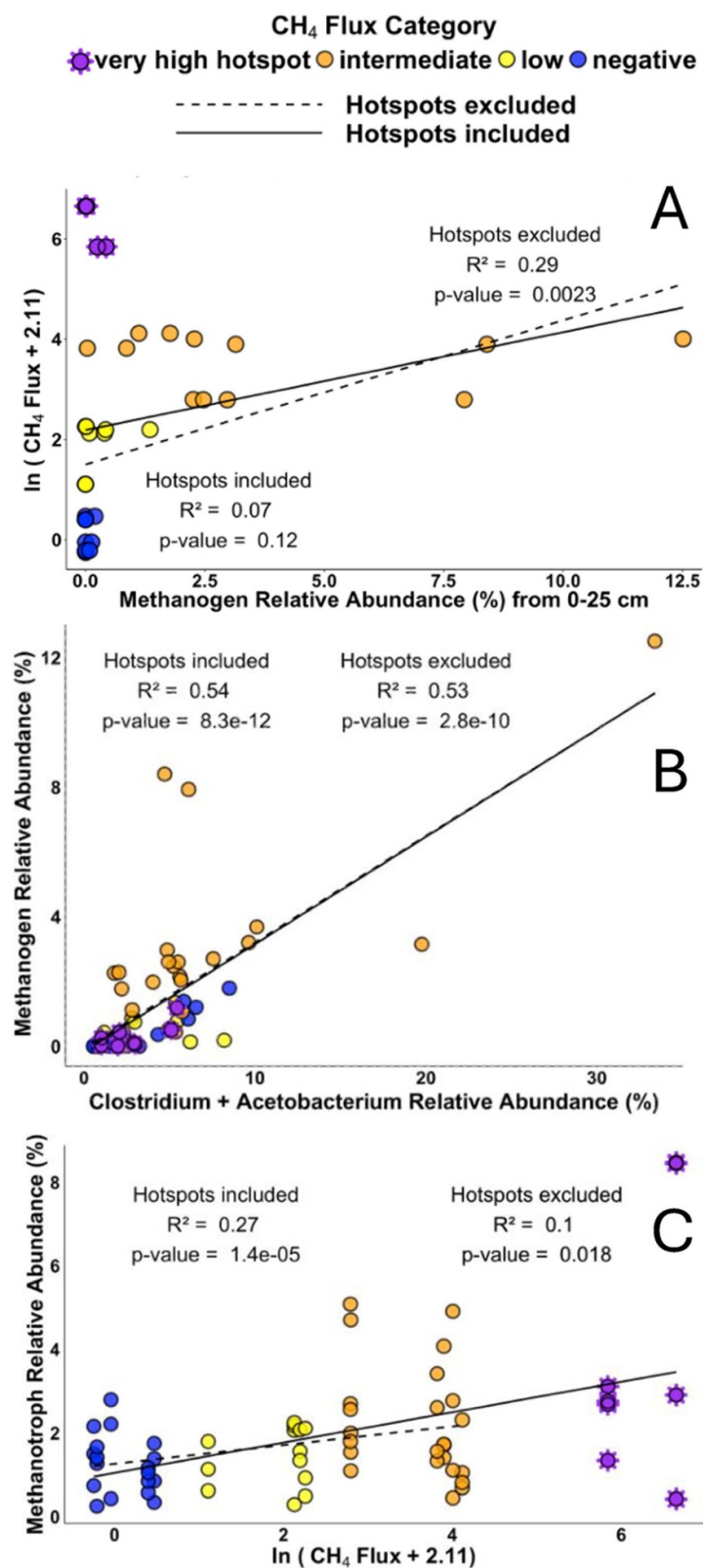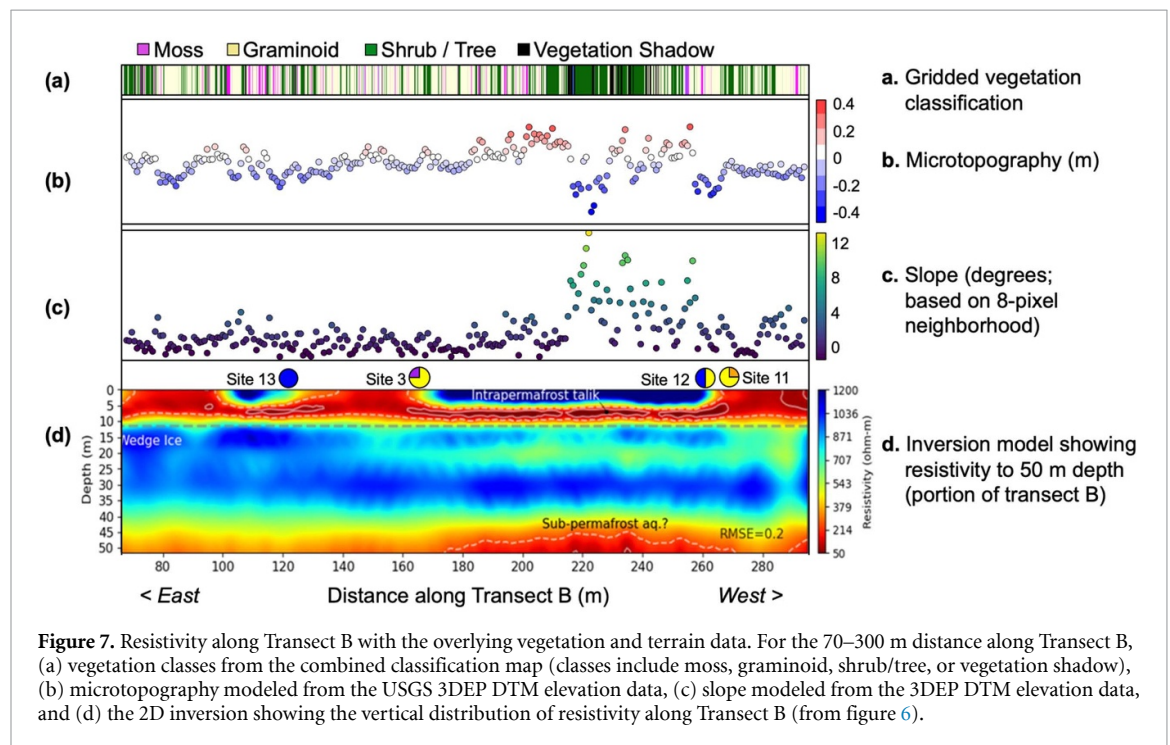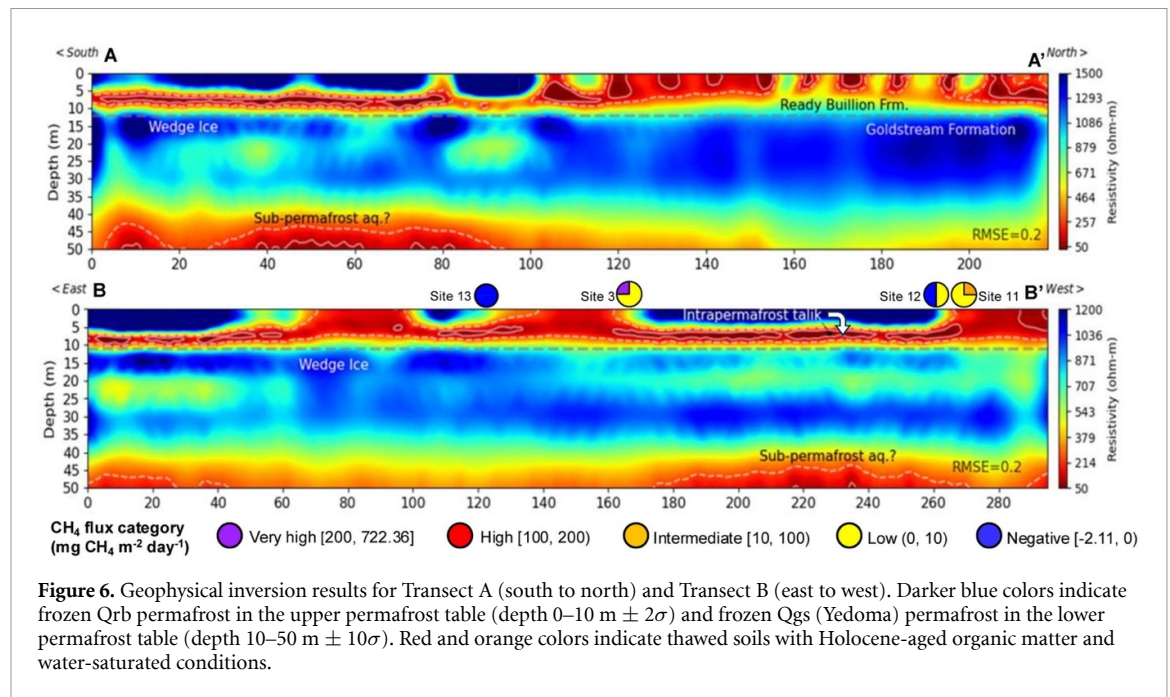
Figure 5. Microbial relative abundance data. Purple stars indicate methane hotspots. Every 'very high' flux site for which we have microbial data was considered a hotspot. (A) Linear regression between methanogen relative abundance in samples collected from 0–25 cm and natural log transformed CH_4 flux. (B) Linear regression between natural log transformed CH_4 flux and methanotroph relative abundance across all samples. (C) Linear regression between methanogen relative abundance and the relative abundance of methanogenic syntrophs *Clostridium* and *Acetobacterium*.

Figure 6. Geophysical inversion results for Transect A (south to north) and Transect B (east to west). Darker blue colors indicate frozen Qrb permafrost in the upper permafrost table (depth 0–10 m $\pm\, 2\sigma$) and frozen Qgs (Yedoma) permafrost in the lower permafrost table (depth 10–50 m $\pm\, 10\sigma$). Red and orange colors indicate thawed soils with Holocene-aged organic matter and water-saturated conditions.

Figure 7. Resistivity along Transect B with the overlying vegetation and terrain data. For the 70–300 m distance along Transect B, (a) vegetation classes from the combined classification map (classes include moss, graminoid, shrub/tree, or vegetation shadow), (b) microtopography modeled from the USGS 3DEP DTM elevation data, (c) slope modeled from the 3DEP DTM elevation data, and (d) the 2D inversion showing the vertical distribution of resistivity along Transect B (from figure 6).

and near-surface drivers. Notably, the relationship between methanogens and their syntrophic partners was evident (figure 5(b)). At thawing-Yedoma sites in Alaska, Walter Anthony *et al* (2024) found that CH_4 flux was weakly related to surface soil moisture and microtopography, and they observed high CH_4 emissions from dry surface soils. Their findings, similar to ours, suggest that wetter conditions in deeper soils facilitate methanogenesis and lead to high CH_4 emissions.

Due to spatiotemporal interactions among temperature, vegetation, soil moisture, and soil

chemistry, it can be difficult to disentangle relationships between CH_4 flux and drivers in observational field studies (Ye *et al* 2012, Turetsky *et al* 2014). We did not observe spatial relationships between CH_4 flux and soil temperature or soil pH, with or without the CH_4 hotspot samples. Similarly, CH_4 flux was not related to air temperature (with or without the hotspot samples). Warmer temperatures might increase both CH_4 production and oxidation, weakening the temperature response of net flux. Soil acidity has been associated with low CH_4 production, but co-varying factors (vegetation, other physicochemical variables)
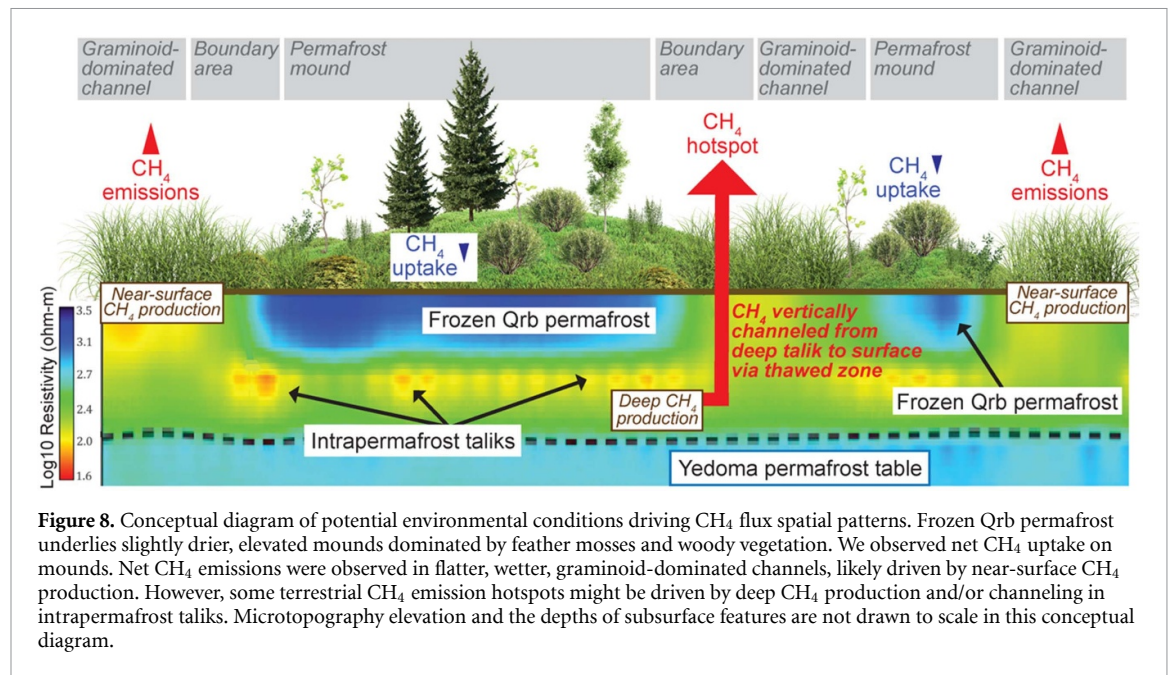
Figure 8. Conceptual diagram of potential environmental conditions driving CH_4 flux spatial patterns. Frozen Qrb permafrost underlies slightly drier, elevated mounds dominated by feather mosses and woody vegetation. We observed net CH_4 uptake on mounds. Net CH_4 emissions were observed in flatter, wetter, graminoid-dominated channels, likely driven by near-surface CH_4 production. However, some terrestrial CH_4 emission hotspots might be driven by deep CH_4 production and/or channeling in intrapermafrost taliks. Microtopography elevation and the depths of subsurface features are not drawn to scale in this conceptual diagram.

might be more important controls on production (Ye *et al* 2012, Wagner *et al* 2017). Additionally, our sampling approach likely did not capture the full spatial variation in CH_4 flux and driver variables across the study area (and did not account for temporal variation), which further limits our ability to observe relationships between CH_4 flux and drivers.

We infer that deep CH_4 production is likely driving some terrestrial hotspot emissions. However, better understanding of the distribution of taliks and permafrost features, and their precise alignment with surface flux data, is needed to support this inference. Moving forward, extensive flux sampling in thawing permafrost environments is needed to understand the spatial distribution of terrestrial CH_4 hotspots. Additionally, our results suggest that talik networks can extend beyond thermokarst lake boundaries in discontinuous permafrost landscapes, and further geophysical surveys are needed to determine talik network extents in the uplands surrounding lakes. Additionally, systems with high SOC, anoxic soils, and hydrological connectivity might transport CH_4 through CH_4-enriched groundwater flow (Paytan *et al* 2015). That is, CH_4 produced in the active layer or in deeper taliks might be transported laterally through groundwater before diffusing upward to the surface. However, with the data generated in this study, we cannot determine whether the observed hotspots were more driven by vertical versus lateral transport of CH_4. Geophysical surveys and groundwater modeling studies might provide insight on the contributions of vertical and lateral transport.

Targeted analyses of subsurface biology and chemistry would help assess the source of CH_4 emitted from hotspots. We describe near-surface soil microbial communities (0–50 cm depth), with a focus on methanogens and their syntrophic partners.

Coring deeper into underlying taliks ($\sim$10 m depth) could identify the communities responsible for the hotspots. Additionally, the observed CH_4 emissions potentially contain mixtures of recently assimilated carbon and older, deeper permafrost carbon. Radiocarbon dating analyses in future studies would provide insight on the relative contributions of near-surface and deeper CH_4 production (e.g. Walter Anthony *et al* 2021). Additionally, isotopic techniques would help to determine the contributions of biogenic versus geologic CH_4 sources to the hotspot emissions (Walter Anthony *et al* 2012, Elder *et al* 2021, Wesley *et al* 2023).

Methane uptake samples had low magnitudes (-2.11 to -0.7 mg CH_4 m^{-2} d^{-1}) but were clustered on small, woody-dominated mounds. The microtopography model illustrates that small mounds occurred across the study area (SI figure 5(c)). This finding provides opportunities for using microtopography models to upscale sink fluxes and estimate their contribution to regional CH_4 budgets. However, further work is needed to assess whether CH_4 sinks are widespread across mounds, and whether this pattern is disrupted by deep thaw-induced CH_4 emission hotspots. More broadly, coarse-scale (1–500 km^2) process models lack representation of fine-scale topography and its influence on CH_4 fluxes (Cresto Aleina *et al* 2015). Similar to Cresto Aleina *et al* (2015), our findings suggest that future efforts should develop methods for parameterizing the effects of fine-scale topography in coarse-scale process models.

Methane emissions are expected to occur in graminoid-dominated, wet fens, yet we observed emission hotspots in drier, moss-dominated areas. Spatial mismatches between surface and subsurface conditions pose a challenge for process-based and statistical CH_4 flux modeling approaches that rely on

surface and near-surface data from optical, thermal infrared, and radar sensors (e.g. land cover data, soil moisture conditions, surface temperature and freeze/thaw status, and active layer dynamics). This highlights the importance of high-resolution (∼5 m) airborne imaging spectroscopy for mapping localized CH_4 concentration hotspots in thawing permafrost environments (Elder *et al* 2021) and the potential for forthcoming spaceborne spectrometer missions to map CH_4 hotspots at regional scales (Bartsch *et al* 2025).

5. Conclusions

Thaw-induced ecosystem changes greatly affect CH_4 fluxes, potentially converting net CH_4 sinks to sources as forests transition to forest-wetland mosaics. However, large uncertainties remain for CH_4 fluxes and their drivers in heterogeneous, transitioning ecosystems, especially regarding the role of deep subsurface conditions. This study assessed surface and near-surface spatial heterogeneity in the context of subsurface permafrost and talik structure, to better understand how these drivers contribute to spatial variation in CH_4 flux. Although it was not possible to conclusively determine the full set of environmental conditions driving CH_4 fluxes, our results suggest that some CH_4 emission hotspots are driven by deep CH_4 production in landscapes with thawing discontinuous permafrost. This study takes an important first step by observing terrestrial CH_4 hotspots in a transitioning forest-fen mosaic and identifying deep permafrost thaw that might contribute to high CH_4 emissions.

Data availability statement

Data for this study is available at https://doi.org/10.3334/ORNLDAAC/2393 (Farina *et al* 2025), including *in situ* data collection, laboratory analysis of soil samples, modeled microtopography and slope data, multispectral drone imagery, and land cover classification. Data on the 16s rRNA gene amplicon sequencing is available through NIH BioProject PRJNA1053625 (www.ncbi.nlm.nih.gov/bioproject/?term=PRJNA1053625) (Christian (2023).

Acknowledgment

Conflict of interest

The authors have no conflict of interest.

ORCID iDs

Mary Farina ⓘ 0000-0003-4163-9989
William Christian ⓘ 0000-0003-1682-8083
Nicholas Hasson ⓘ 0000-0003-2351-8358
Timothy McDermott ⓘ 0000-0001-8293-5106
Scott Powell ⓘ 0000-0002-5752-0408
Roland Hatzenpichler ⓘ 0000-0002-5489-3444
Hailey Webb ⓘ 0000-0002-5500-0214
Eric A Sproles ⓘ 0000-0003-1245-1653

References

Andersen R, Chapman S J and Artz R R E 2013 Microbial communities in natural and disturbed peatlands: a review *Soil Biol. Biochem.* **57** 979–94

Bao T, Jia G and Xu X 2021 Wetland heterogeneity determines methane emissions: a pan-arctic synthesis *Environ. Sci. Technol.* **55** 10152–63

Bartsch A *et al* 2025 Advancing the Arctic methane permafrost challenge (AMPAC) with future satellite missions *IEEE J. Sel. Top. Appl. Earth Obs. Remote Sens.* **18** 6279–98

Benson A K, Payne K L and Stubben M A 1997 Mapping groundwater contamination using dc resistivity and VLF geophysical methods–a case study *Geophysics* **62** 80–86

Bolyen E *et al* 2019 Reproducible, interactive, scalable and extensible microbiome data science using QIIME 2 *Nat. Biotechnol.* **37** 852–7

Bourgeau-Chavez L L, Bosse K R, Poley A F and Battaglia M J 2025 *ABoVE: Soil Moisture and ALT Field Collection Protocols and Probe Calibration* (ORNL DAAC) (https://doi.org/10.3334/ORNLDAAC/2373)

Bruhwiler L, Parmentier F-J W, Crill P, Leonard M and Palmer P I 2021 The Arctic carbon cycle and its response to changing climate *Curr. Clim. Change Rep.* **7** 14–34

Bubier J, Costello A, Moore T R, Roulet N T and Savage K 1993 Microtopography and methane flux in boreal peatlands, northern Ontario, Canada *Can. J. Bot.* **71** 1056–63

Callahan B J, McMurdie P J, Rosen M J, Han A W, Johnson A J A and Holmes S P 2016 DADA2: high-resolution sample inference from Illumina amplicon data *Nat. Methods* **13** 581–3

Chapman E J, Cadillo-Quiroz H, Childers D L, Turetsky M R and Waldrop M P 2017 Soil microbial community composition is correlated to soil carbon processing along a boreal wetland formation gradient *Eur. J. Soil Biol.* **82** 17–26

Christian W 2023 Alaska Permafrost Soil Community *BioProject* (available at: www.ncbi.nlm.nih.gov/bioproject/1053625)

Constable S C, Parker R L and Constable C G 1987 Occam's inversion: a practical algorithm for generating smooth

models from electromagnetic sounding data *Geophysics* **52** 289–300

Cresto Aleina F, Runkle B R, Kleinen T, Kutzbach L, Schneider J and Brovkin V 2015 Modeling micro-topographic controls on boreal peatland hydrology and methane fluxes *Biogeosciences* **12** 5689–704

Davis N M, Proctor D M, Holmes S P, Relman D A and Callahan B J 2018 Simple statistical identification and removal of contaminant sequences in marker-gene and metagenomics data *Microbiome* **6** 226

deGroot-Hedlin C and Constable S 1990 Occam's inversion to generate smooth, two-dimensional models from magnetotelluric data *Geophysics* **55** 1613–24

Dorodnikov M, Marushchak M, Biasi C and Wilmking M 2013 Effect of microtopography on isotopic composition of methane in porewater and efflux at a boreal peatland *Boreal Environ. Res.* **18** 269–79

Dorrepaal E, Toet S, Van Logtestijn R S P, Swart E, Van De Weg M J, Callaghan T V and Aerts R 2009 Carbon respiration from subsurface peat accelerated by climate warming in the subarctic *Nature* **460** 616–9

Douglas T A, Jorgenson M T, Brown D R N, Campbell S W, Hiemstra C A, Saari S P, Bjella K and Liljedahl A K 2016 Degrading permafrost mapped with electrical resistivity tomography, airborne imagery and LiDAR, and seasonal thaw measurements *Geophysics* **81** WA71–85

Douglas T A, Turetsky M R and Koven C D 2020 Increased rainfall stimulates permafrost thaw across a variety of Interior Alaskan boreal ecosystems *npj Clim. Atmos. Sci.* **3** 28

Dubey M, Hadadi N, Pelet S, Carraro N, Johnson D R and van der Meer J R 2021 Environmental connectivity controls diversity in soil microbial communities *Commun. Biol.* **4** 492

Dunfield P, Knowles R, Dumont R and Moore T 1993 Methane production and consumption in temperate and subarctic peat soils: response to temperature and pH *Soil Biol. Biochem.* **25** 321–6

Elder C D *et al* 2021 Characterizing methane emission hotspots from thawing permafrost *Glob. Biogeochem. Cycles* **35** e2020GB006922

Farina M, Christian W, Watts J, McDermott T, Hatzenpichler R, LaRue G, Powell S, Webb H, Barnes N and Okano K 2025 ABoVE: Land Cover, Methane Flux, and Environmental Data, Big Trail Lake, Fairbanks AK *ORNL DAAC* (https://doi.org/10.3334/ORNLDAAC/2393)

Farquharson L M, Romanovsky V E, Kholodov A and Nicolsky D 2022 Sub-aerial talik formation observed across the discontinuous permafrost zone of Alaska *Nat. Geosci.* **15** 475–81

Fofana A *et al* 2022 Mapping substrate use across a permafrost thaw gradient *Soil Biol. Biochem.* **175** 108809

Frenzel P and Karofeld E 2000 CH4 emission from a hollow-ridge complex in a raised bog: the role of CH4 production and oxidation *Biogeochemistry* **51** 91–112

Galand P E, Fritze H and Yrjälä K 2003 Microsite-dependent changes in methanogenic populations in a boreal oligotrophic fen *Environ. Microbiol.* **5** 1133–43

Galand P E, Saarnio S, Fritze H and Yrjã¤lã¤ K 2002 Depth related diversity of methanogen Archaea in Finnish oligotrophic fen *FEMS Microbiol. Ecol.* **42** 441–9

Graham J D, Ricciuto D M, Glenn N F and Hanson P J 2022 Incorporating microtopography in a land surface model and quantifying the effect on the carbon cycle *J. Adv. Model. Earth Syst.* **14** e2021MS002721

Hamilton T D, Craig J L and Sellmann P V 1988 The Fox permafrost tunnel: a late Quaternary geologic record in central Alaska *GSA Bulletin* **100** 6

Helbig M, Chasmer L E, Desai A R, Kljun N, Quinton W L and Sonnentag O 2017 Direct and indirect climate change effects on carbon dioxide fluxes in a thawing boreal forest–wetland landscape *Glob. Change Biol.* **23** 3231–48

Hoekstra P, Sellmann P V and Delaney A J 1974 *Airborne Resistivity Mapping of Permafrost near Fairbanks, Alaska* (Cold Regions Research and Engineering Laboratory)

Hoekstra P, Sellmann P V and Delaney A 1975 Ground and airborne resistivity surveys of permafrost near Fairbanks, Alaska *Geophysics* **40** 641–56

Hugelius G *et al* 2024 Permafrost region greenhouse gas budgets suggest a weak CO_2 sink and CH_4 and N_2O sources, but magnitudes differ between top-down and bottom-up methods *Glob. Biogeochem. Cycles* **38** e2023GB007969

James S R, Minsley B J, McFarland J W, Euskirchen E S, Edgar C W and Waldrop M P 2021 The biophysical role of water and ice within permafrost nearing collapse: insights from novel geophysical observations *J. Geophys. Res. Earth Surf.* **126** e2021JF006104

Jorgenson M T and Osterkamp T E 2005 Response of boreal ecosystems to varying modes of permafrost degradation *Can. J. For. Res.* **35** 2100–11

Juottonen H, Kotiaho M, Robinson D, Merilä P, Fritze H, Tuittila E-S and King G 2015 Microform-related community patterns of methane-cycling microbes in boreal Sphagnum bogs are site specific *FEMS Microbiol. Ecol.* **91** fiv094

Kanevskiy M, Shur Y, Bigelow N H, Bjella K L, Douglas T A, Fortier D, Jones B M and Jorgenson M T 2022 Yedoma cryostratigraphy of recently excavated sections of the CRREL permafrost tunnel near fairbanks, Alaska *Front. Earth Sci.* **9** 758800

Kolb S 2009 The quest for atmospheric methane oxidizers in forest soils *Environ. Microbiol. Rep.* **1** 336–46

Krukenberg V, Reichart N J, Spietz R L and Hatzenpichler R 2021 Microbial community response to polysaccharide amendment in anoxic hydrothermal sediments of the guaymas basin *Front. Microbiol.* **12** 763971

Kuhn M A, Varner R K, Bastviken D, Crill P, MacIntyre S, Turetsky M, Walter Anthony K, McGuire A D and Olefeldt D 2021 BAWLD-CH 4: a comprehensive dataset of methane fluxes from boreal and arctic ecosystems *Earth Syst. Sci. Data Discuss.* **13** 5151–89

Kwon M J, Jung J Y, Tripathi B M, Göckede M, Lee Y K and Kim M 2019 Dynamics of microbial communities and CO_2 and CH_4 fluxes in the tundra ecosystems of the changing Arctic *J. Microbiol.* **57** 325–36

Lara M J, Genet H, McGuire A D, Euskirchen E S, Zhang Y, Brown D R N, Jorgenson M T, Romanovsky V, Breen A and Bolton W R 2016 Thermokarst rates intensify due to climate change and forest fragmentation in an Alaskan boreal forest lowland *Glob. Change Biol.* **22** 816–29

Liljedahl A K, Timling I, Frost G V and Daanen R P 2020 Arctic riparian shrub expansion indicates a shift from streams gaining water to those that lose flow *Commun Earth Environ* **1** 50

Masson-Delmotte V P, Zhai P, Pirani S L, Connors C, Péan S, Berger N, Caud Y, Chen L, Goldfarb M I and Scheel Monteiro P M 2021 Summary for policymakers *Climate Change 2021: The Physical Science Basis. Contribution of Working Group I to the Sixth Assessment Report of the Intergovernmental Panel on Climate Change* (IPCC)

McNeill J D and Labson V F 1991 Geological mapping using VLF radio fields

Monteiro Santos F A 2004 1-D laterally constrained inversion of EM34 profiling data *J. Appl. Geophys.* **56** 123–34

Myhre G, Shindell D, Bréon F M, Collins W, Fuglestvedt J, Huang J, Koch D, Lamarque J F, Lee D and Mendoza B 2014 Anthropogenic and natural radiative forcing *Climate Change 2013-The Physical Science Basis* (Cambridge University Press) pp 659–740

O'Neill H B, Roy-Leveillee P, Lebedeva L and Ling F 2020 Recent advances (2010–2019) in the study of taliks *Permafr. Periglac. Process.* **31** 346–57

OCM Partners 2023 2017 USGS 3DEP Lidar: Fairbanks, AK (QL1 & QL2) (NOAA National Centers for Environmental Information) (available at: www.fisheries.noaa.gov/inport/item/55358)

Oh Y *et al* 2020 Reduced net methane emissions due to microbial methane oxidation in a warmer Arctic *Nat. Clim. Change* **10** 317–21

Olefeldt D, Hovemyr M, Kuhn M A, Bastviken D, Bohn T J, Connolly J, Crill P, Euskirchen E S, Finkelstein S A and Genet H 2021 The boreal-arctic wetland and lake dataset (BAWLD) *Earth Syst. Sci. Data Discuss.* **13** 5127–49

Olefeldt D, Turetsky M R, Crill P M and McGuire A D 2013 Environmental and physical controls on northern terrestrial methane emissions across permafrost zones *Glob. Change Biol.* **19** 589–603

Osterkamp T E, Viereck L, Shur Y, Jorgenson M T, Racine C, Doyle A and Boone R D 2000 Observations of thermokarst and its impact on boreal forests in Alaska, U.S.A *Arct. Antarct. Alp. Res.* **32** 303–15

Parada A E, Needham D M and Fuhrman J A 2016 Every base matters: assessing small subunit rRNA primers for marine microbiomes with mock communities, time series and global field samples *Environ. Microbiol.* **18** 1403–14

Paytan A, Lecher A L, Dimova N, Sparrow K J, Kodovska F G-T, Murray J, Tulaczyk S and Kessler J D 2015 Methane transport from the active layer to lakes in the Arctic using Toolik Lake, Alaska, as a case study *Proc. Natl Acad. Sci.* **112** 3636–40

Peltoniemi K *et al* 2016 Responses of methanogenic and methanotrophic communities to warming in varying moisture regimes of two boreal fens *Soil Biol. Biochem.* **97** 144–56

Péwé T L 1958 *Geology of the Fairbanks (D-2) Quadrangle, Alaska* (US Geological Survey)

Péwé T L 1975a *Quaternary Stratigraphic Nomenclature in Unglaciated Central Alaska* (US Government Publishing Office)

Péwé T L 1975b *Quaternary Geology of Alaska* vol 835 (US Government Printing Office)

Ping C-L, Boone R D, Clark M H, Packee E C and Swanson D K 2006 State factor control of soil formation in interior Alaska *Alaska's Changing Boreal Forest* pp 21–38

Quast C, Pruesse E, Yilmaz P, Gerken J, Schweer T, Yarza P, Peplies J and Glöckner F O 2012 The SILVA ribosomal RNA gene database project: improved data processing and web-based tools *Nucleic Acids Res.* **41** D590–6

Rantanen M, Karpechko A Y, Lipponen A, Nordling K, Hyvärinen O, Ruosteenoja K, Vihma T and Laaksonen A 2022 The Arctic has warmed nearly four times faster than the globe since 1979 *Commun. Earth Environ.* **3** 168

Rodenhizer H, Belshe F, Celis G, Ledman J, Mauritz M, Goetz S, Sankey T and Schuur E A G 2022 Abrupt permafrost thaw accelerates carbon dioxide and methane release at a tussock tundra site *Arct. Antarct. Alp. Res.* **54** 443–64

Rupp D, Kane E S, Dieleman C, Keller J K and Turetsky M 2019 Plant functional group effects on peat carbon cycling in a boreal rich fen *Biogeochemistry* **144** 305–27

Sasaki Y 1989 Two-dimensional joint inversion of magnetotelluric and dipole-dipole resistivity data *Geophysics* **54** 254–62

Sasaki Y 2001 Full 3D inversion of electromagnetic data on PC *J. Appl. Geophys.* **46** 45–54

Saunois M, Stavert A R, Poulter B, Bousquet P, Canadell J G, Jackson R B, Raymond P A, Dlugokencky E J, Houweling S and Patra P K 2020 The global methane budget 2000–2017 *Earth Syst. Sci. Data Discuss.* **12** 1561–623

Schuur E A G *et al* 2015 Climate change and the permafrost carbon feedback *Nature* **520** 171–9

Sellmann P V 1967 Geology of the USA CRREL permafrost tunnel, Fairbanks, Alaska

Shcherbakova V A, Chuvilskaya N A, Rivkina E M, Pecheritsyna S A, Laurinavichius K S, Suzina N E, Osipov G A, Lysenko A M, Gilichinsky D A and Akimenko V K 2005 Novel psychrophilic anaerobic spore-forming bacterium from the overcooled water brine in permafrost: description Clostridium algoriphilum sp. nov *Extremophiles* **9** 239–46

Soil Survey Staff, Natural Resources Conservation Service, United States Department of Agriculture Official soil series

descriptions (available at: https://casoilresource.lawr. ucdavis.edu/sde/?series=goldstream#osd) (Accessed 2 October 2023)

Stewart M and Bretnall R 1986 Interpretation of VLF resistivity data for ground water contamination surveys *Ground Water Monit. Remediat.* **6** 71–75

Thompson L R *et al* 2017 A communal catalogue reveals Earth's multiscale microbial diversity *Nature* **551** 457–463

Treat C C *et al* 2015 A pan-Arctic synthesis of CH_4 and CO_2 production from anoxic soil incubations *Glob. Change Biol.* **21** 2787–803

Turetsky M R *et al* 2014 A synthesis of methane emissions from 71 northern, temperate, and subtropical wetlands *Glob. Change Biol.* **20** 2183–97

Turetsky M R *et al* 2020 Carbon release through abrupt permafrost thaw *Nat. Geosci.* **13** 138–43

Turetsky M R, Treat C C, Waldrop M P, Waddington J M, Harden J W and McGuire A D 2008 Short-term response of methane fluxes and methanogen activity to water table and soil warming manipulations in an Alaskan peatland *J. Geophys. Res. Biogeosci.* **113** 2007JG000496

Tveit A T, Urich T, Frenzel P and Svenning M M 2015 Metabolic and trophic interactions modulate methane production by Arctic peat microbiota in response to warming *Proc. Natl Acad. Sci.* **112** E2507–16

Wagg C, Hautier Y, Pellkofer S, Banerjee S, Schmid B and Van Der Heijden M G 2021 Diversity and asynchrony in soil microbial communities stabilizes ecosystem functioning *elife* **10** e62813

Wagner R, Zona D, Oechel W and Lipson D 2017 Microbial community structure and soil p H correspond to methane production in A rctic A laska soils *Environ. Microbiol.* **19** 3398–410

Waldrop M P *et al* 2021 Carbon fluxes and microbial activities from boreal peatlands experiencing permafrost thaw *J. Geophys. Res. Biogeosci.* **126** e2020JG005869

Walter Anthony K M *et al* 2021 Decadal-scale hotspot methane ebullition within lakes following abrupt permafrost thaw *Environ. Res. Lett.* **16** 035010

Walter Anthony K M *et al* 2024 Upland Yedoma taliks are an unpredicted source of atmospheric methane *Nat. Commun.* **15** 6056

Walter Anthony K M, Anthony P, Grosse G and Chanton J 2012 Geologic methane seeps along boundaries of Arctic permafrost thaw and melting glaciers *Nat. Geosci.* **5** 419–26

Walvoord M A and Kurylyk B L 2016 Hydrologic impacts of thawing permafrost—a review *Vadose Zone J.* **15** 1–20

Wang Y *et al* 2024 Intensified positive Arctic–Methane feedback under IPCC climate scenarios in the 21st Century *Ecosyst. Health Sustain.* **10** 0185

Watts J D *et al* 2023 Carbon uptake in Eurasian boreal forests dominates the high-latitude net ecosystem carbon budget *Glob. Change Biol.* **29** 1870–89

Wendler G and Shulski M 2009 A century of climate change for Fairbanks, Alaska *Arctic* **62** 295–300

Wesley D, Dallimore S, MacLeod R, Sachs T and Risk D 2023 Characterization of atmospheric methane release in the outer Mackenzie River delta from biogenic and thermogenic sources *The Cryosphere* **17** 5283–97

Wright S N, Thompson L M, Olefeldt D, Connon R F, Carpino O A, Beel C R and Quinton W L 2022 Thaw-induced impacts on land and water in discontinuous permafrost: a review of the Taiga Plains and Taiga Shield, northwestern Canada *Earth Sci. Rev.* **232** 104104

Ye R, Jin Q, Bohannan B, Keller J K, McAllister S A and Bridgham S D 2012 pH controls over anaerobic carbon mineralization, the efficiency of methane production, and methanogenic pathways in peatlands across an ombrotrophic–minerotrophic gradient *Soil Biol. Biochem.* **54** 36–47

Yilmaz P, Parfrey L W, Yarza P, Gerken J, Pruesse E, Quast C, Schweer T, Peplies J, Ludwig W and Glöckner F O 2014 The

SILVA and "All-species Living Tree Project (LTP)" taxonomic frameworks *Nucleic Acids Res.* **42** D643–8

Ying Q, Poulter B, Watts J D, Arndt K A, Virkkala A M, Bruhwiler L and Zhang Z 2024 WetCH$_4$: a machine learning-based upscaling of methane fluxes of Northern Wetlands during 2016–2022 *Earth Syst. Sci. Data Discuss.* **17** 2507–34

Zhang H *et al* 2021 Methane production and oxidation potentials along a fen-bog gradient from southern boreal to subarctic peatlands in Finland *Glob. Change Biol.* **27** 4449–64

Zhang Z, Zimmermann N E, Stenke A, Li X, Hodson E L, Zhu G, Huang C and Poulter B 2017 Emerging role of wetland methane emissions in driving 21st century climate change *Proc. Natl Acad. Sci.* **114** 9647–52